

Reconstruction of steps on the Cu(111) surface induced by sulfur

Holly Walen,^{1,a)} Da-Jiang Liu,² Junepyo Oh,³ Hyunseob Lim,^{3,b)} J. W. Evans,^{2,4} Yousoo Kim,³ and P. A. Thiel^{1,2,5}

¹Department of Chemistry, Iowa State University, Ames, Iowa 50011, USA

²Ames Laboratory of the USDOE, Ames, Iowa 50011, USA

³RIKEN Surface and Interface Science Laboratory, Wako, Saitama 351-0198, Japan

⁴Department of Physics and Astronomy, Iowa State University, Ames, Iowa 50011, USA

⁵Department of Materials Science and Engineering, Iowa State University, Ames, Iowa 50011, USA

(Received 18 February 2015; accepted 6 May 2015; published online 21 May 2015)

A rich menagerie of structures is identified at 5 K following adsorption of low coverages (≤ 0.05 monolayers) of S on Cu(111) at room temperature. This paper emphasizes the reconstructions at the steps. The A-type close-packed step has 1 row of S atoms along its lower edge, where S atoms occupy alternating pseudo-fourfold-hollow (p4fh) sites. Additionally, there are 2 rows of S atoms of equal density on the upper edge, bridging a row of extra Cu atoms, together creating an extended chain. The B-type close-packed step exhibits an even more complex reconstruction, in which triangle-shaped groups of Cu atoms shift out of their original sites and form a base for S adsorption at (mostly) 4fh sites. We propose a mechanism by which these triangles could generate Cu–S complexes and short chains like those observed on the terraces. © 2015 AIP Publishing LLC. [<http://dx.doi.org/10.1063/1.4921258>]

I. INTRODUCTION

Because of the low coordination of atoms at surface steps, steps are important active sites in many surface processes, from heterogeneous catalysis,¹ to thin film growth,² to oxidation.³ They often serve as a dynamic reservoir of atoms in cases where the surface itself is a reactant. The signature of such a reaction can be etching, recession, and/or faceting of the steps. For example, Ruan *et al.* showed that sulfur-induced reconstruction on Cu(111) is accompanied by step recession at room temperature and concluded that Cu is incorporated into the reconstructed phase.⁴

There is mounting evidence that metal atoms react with sulfur or sulfur-containing molecules to form localized complexes on surfaces of the coinage metals.^{5–7} (Molecules with some other functional groups, such as cyano groups, can also self-metallate on these surfaces.^{8,9}) Sulfur on Cu(111) is one such system. On Cu(111), Feibelman first proposed a Cu₃S₃ complex as an agent of mass transport on the basis of density functional theory (DFT).^{10,11} It is a triangle of Cu atoms, decorated by nearly coplanar S atoms at its edges. Its stability was attributed to the fact that S is in pseudo-fourfold-hollow (p4fh) sites, which are more favorable for S adsorption than the three-fold hollow (3fh) sites present on the terraces. This is in accord with a long-standing principle that high-coordination sites, such as 4fh sites, stabilize adsorbed S and are created in some S-induced reconstructions.^{10,12,13} Recently, we identified a different complex, heart-shaped Cu₂S₃, as the dominant terrace species at very low sulfur coverage and very low temperature (5 K), based on scanning tunneling microscopy (STM) and DFT.¹⁴ We proposed that the Cu₂S₃ species owes

its stability to the linearity of its S–Cu–S subunits, in addition to the presence of one S adatom at a p4fh site.

There have been a number of other studies of S on Cu(111).^{4,12,15–21} The work most relevant to the current study is that of Wahlström *et al.*,^{20,21} who characterized this system at temperatures down to 50 K and discovered a number of low-temperature ordered phases. The lowest-coverage phase was a $(\sqrt{43} \times \sqrt{43})$ R $\pm 7.5^\circ$ (hereafter referred to as $\sqrt{43}$) reconstruction with an ideal coverage of 0.27 monolayers (ML) and a disordering temperature of 170 K. We recently re-examined the structure of this phase and proposed a model that is not related in any straightforward way either to bulk CuS (the original model²¹) or to the Cu₂S₃ (or Cu₃S₃) complex.²² Additionally, Wahlström *et al.* observed pronounced triangular features at some step edges.

In this paper, we find that sulfur induces complex reconstructions of the steps, which we identify on the basis of STM and DFT. The paper is organized as follows. Section II provides experimental and computational details, Secs. III and IV present experimental and computational results, respectively, and Sec. V is a discussion of the results.

II. EXPERIMENTAL AND COMPUTATIONAL DETAILS

A. Experimental description

All STM imaging was done at 5 K with a low-temperature STM (LT-STM Omicron GmbH) in a UHV chamber with base pressure below 2.5×10^{-11} Torr. Images were obtained using a W tip. In an adjacent chamber, the Cu(111) sample was cleaned. Each cleaning cycle consisted of several steps: (1) heating the sample at 820 K for 5 min; (2) sputtering with Ar⁺ (12 μA, 2.0 kV) at 820 K for 10 min; (3) continuing to sputter for 2 min while the sample cooled; and (4) flashing back to 800 K without sputtering. Cleaning between experiments

^{a)}Author to whom correspondence should be addressed. Electronic mail: hwalen@iastate.edu

^{b)}Current address: Ulsan National Institute of Science and Technology, South Korea.

consisted of two to three such cycles. Sample temperatures during cleaning were measured with an optical pyrometer, for which the uncertainty was estimated as ± 10 K, based on variation of the reading with the emission angle.

The adjacent chamber also contained the sulfur source, a solid-state electrochemical Ag|AgI|Ag₂S|Pt cell.²³ To generate sulfur, the Pt cathode was biased at 0.20–0.25 V with respect to the Ag anode and the cell was heated independently. The cell temperature was recorded via a thermocouple located near, but not in direct contact, with the chemical components of the cell. The thermocouple reading corresponded to a temperature of 160 °C during cell operation. Work by Detry *et al.* indicates that these conditions of cell operation produce mainly S₂ (gas).²⁴ We verified the production of sulfur by measuring a mass spectrum with the evaporator running and observing peaks at mass-to-charge ratios of 32 and 64.

During sulfur deposition, the sample was held at room temperature to ensure dissociative adsorption.²⁵ The sample was then transferred into the STM stage and cooled to the imaging temperature, 5 K. Typical tunneling conditions were -1.0 V to $+1.0$ V sample bias (V_S) and 0.3 – 1.5 nA tunneling current (I). We have carefully analyzed the way in which topographic heights and widths of the terrace hearts depend upon tunneling parameters within this range of voltages and currents. There is no statistically significant trend. This, plus our experience in imaging diverse features in other S adsorption systems, leads us to conclude that there is no significant effect of tunneling conditions (within this range) on the step features either. Exact tunneling conditions for each individual image can be found in the supplementary material.³³

By scanning over the same region several times, we determined that the structures were immobile and stable under these experimental conditions. In all experiments, the sample was first imaged at 5 K after sulfur deposition, and then it was re-heated to room temperature and re-cooled for imaging. This treatment had no effect on the observed structures or their populations. The sample had the same azimuthal orientation relative to the image frame in all experiments, so orientations of features can be compared directly between all STM images, with the exception of Figs. 13 and 14 where STM images have been rotated to facilitate visual comparison with a model.

The STM piezoelectric calibration was checked by measuring a , the atomic separation along close-packed directions [Fig. 1(a)], and by measuring step heights (not shown). The former value was 0.250 ± 0.005 nm, and the latter was 0.19 ± 0.02 nm. Within the stated uncertainties, these equal the bulk parameters of 0.255 nm and 0.208 nm, respectively. Thus, the calibration was validated. Constant-current STM images are referred to as topographic images. These are presented after minimal correction—planning and flattening—using WSxM software.²⁶

Areal coverage was determined by using the flooding function in WSxM software²⁶ to determine the area of all Cu–S species on the terraces and then dividing by the total image area. Step edges were omitted from this calculation. The areal coverages ranged from 0.010 to 0.125. We determined an approximate absolute coverage by referring to previous work by Wahlström *et al.*, where islands of the Cu–S $\sqrt{43}$ reconstruction were reported to form at $\theta_S \sim 0.05$.^{20,21} This

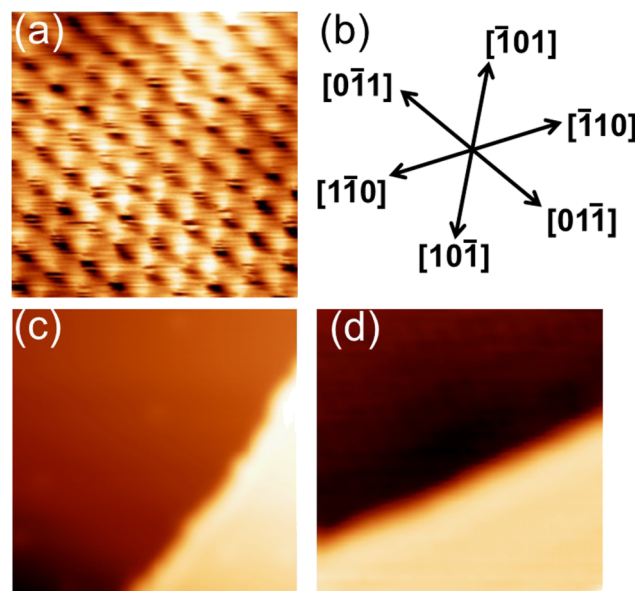


FIG. 1. Features of the clean Cu(111) surface. (a) Atomically resolved STM image, 2.0×2.0 nm². (b) Close-packed directions. (c) Clean, 10×10 nm². (d) Clean step, 10×10 nm².

occurred at our highest areal coverage of 0.125, so the absolute coverage is roughly 2/5 the areal coverage. Applying this constant to the rest of the areal coverage range, the range of absolute S coverage (θ_S) is approximately 0.004 ML–0.050 ML, where $\theta_S = 1$ (or a coverage of 1 ML) is defined as a ratio of 1 S atom to 1 Cu atom in the Cu(111) plane.

B. Computational description

The computational approach has been described elsewhere.¹⁴ Energetics are obtained by averaging calculations on 4–7 layer slabs of Cu(111) to minimize the impact of surface states.²⁷ Error bars in graphs, or numerical uncertainties in parentheses, are derived from the range of values for different slab thicknesses.²⁷ Most of the results shown here used “high” k-point grids corresponding approximately to $(24 \times 24 \times 1)$ for the primitive cell and have uncertainties of 5–8 meV. Some results in the Appendix used a “low” k-points grid corresponding to $(12 \times 12 \times 1)$ for the primitive cell and have higher uncertainties of 10–20 meV. Images with a periodic arrangement are (2×2) or (3×2) representations of the original supercells. All models of DFT configurations show the energy-optimized atomic coordinates. In energy optimization, the bottom layer of Cu in the slab was fixed at bulk positions with theoretical bulk lattice constant, and all other atoms were allowed to relax. STM images were simulated from DFT using the Tersoff-Hamann²⁸ method, which essentially generates the electron isodensity contour surface at the Fermi edge.

III. EXPERIMENTAL RESULTS

A. Overview of features on terraces and steps

Figure 1(a) is an image of the clean Cu(111) surface with atomic resolution. Consequently, close-packed crystallographic directions are identified in Fig. 1(b). Figures 1(c) and

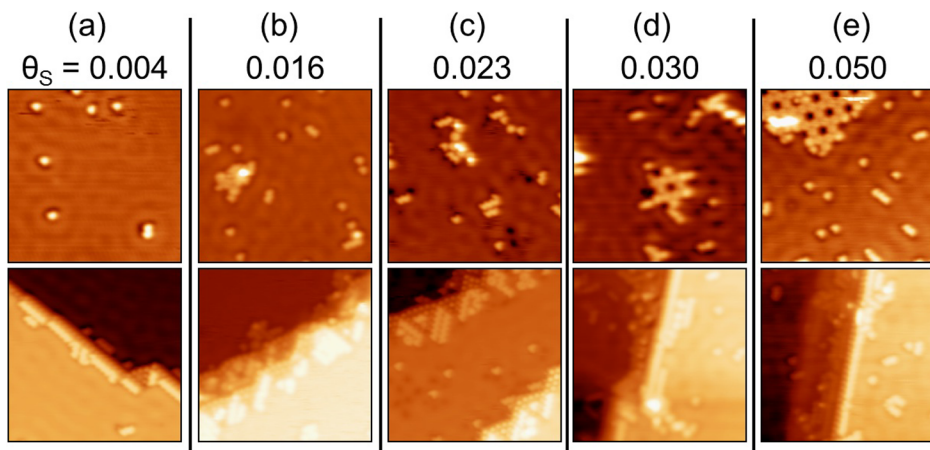


FIG. 2. STM topographic images in order of increasing sulfur coverage, θ_S . All images are $15 \times 15 \text{ nm}^2$.

1(d) are examples of step edges on the clean surface. The step in Fig. 1(d) is nearly parallel to a close-packed direction and hence is very smooth, while that in Fig. 1(c) lies between two close-packed directions and is slightly rough, presumably due to kinks.

Figure 2 shows Cu(111) terraces (top panels) and steps (bottom panels), at $\theta_S = 0.004\text{--}0.050$. At the lowest coverage, the main features on the terraces are small, uniform bright spots that are the heart-shaped Cu_2S_3 complexes discussed elsewhere¹⁴ [Fig. 2(a)]. Close views and schematics of three such complexes are shown in Figs. 3(a), 3(b), and 3(e). Even at this low coverage, step edges are heavily decorated.

At $\theta_S = 0.016$, short linear chains appear on the terraces, resembling concatenations of hearts [Fig. 2(b)]. Two high-magnification examples of linear chains, and corresponding models, are shown in Figs. 3(c) and 3(d). The arrangements are built from Cu_2S_3 complexes that condense by sharing S atoms. Linear chains observed on the terraces tend to be short, only 2 to 5 units long; linear chains near steps can be much longer, up to 23 units. The spacing between lobes (S atoms) in the middle of the chain should be $2a = 0.51 \text{ nm}$, according to the models of Figs. 3(c) and 3(d). This is exactly the value measured from STM images, $0.51 \pm 0.03 \text{ nm}$ (for sample size $N = 63$).

By $\theta_S = 0.023$, clump-like features also appear on the terraces. Some consist of hearts or chains, as shown in Fig. 3(e). In others, hearts or chains make only a minor contribution, or are not identifiable at all, as in Fig. 3(f).

At $\theta_S = 0.030$, terraces contain small fragments of the $\sqrt{43}$ reconstruction, such as the individual dark spot encircled by tendrils in Fig. 2(d). At $\theta_S = 0.050$, clear islands of $\sqrt{43}$ appear, as shown in Fig. 2(e). The $\sqrt{43}$ is identified on the basis of its honeycomb pattern of dark spots,^{20–22} together with its unit cell length and orientation.

The observations of the Cu–S complexes and $\sqrt{43}$ reconstruction on the terraces help to define the conditions under which the intricate step structures form.

B. STM examination of features at and near step edges

1. Identification of A- and B-steps

On a fcc(111) surface, there are two types of close-packed step edges, denoted A and B.²⁹ The A-step consists of p4fh

sites, and the B-step consists of pseudo-threefold (p3fh) sites. A- and B-steps are difficult to distinguish on the clean surface, but we will show that they can be differentiated on Cu(111) based on their response to S adsorption.

We begin with an experiment in which θ_S is so low that there are no S-induced features on terraces, i.e., lower than

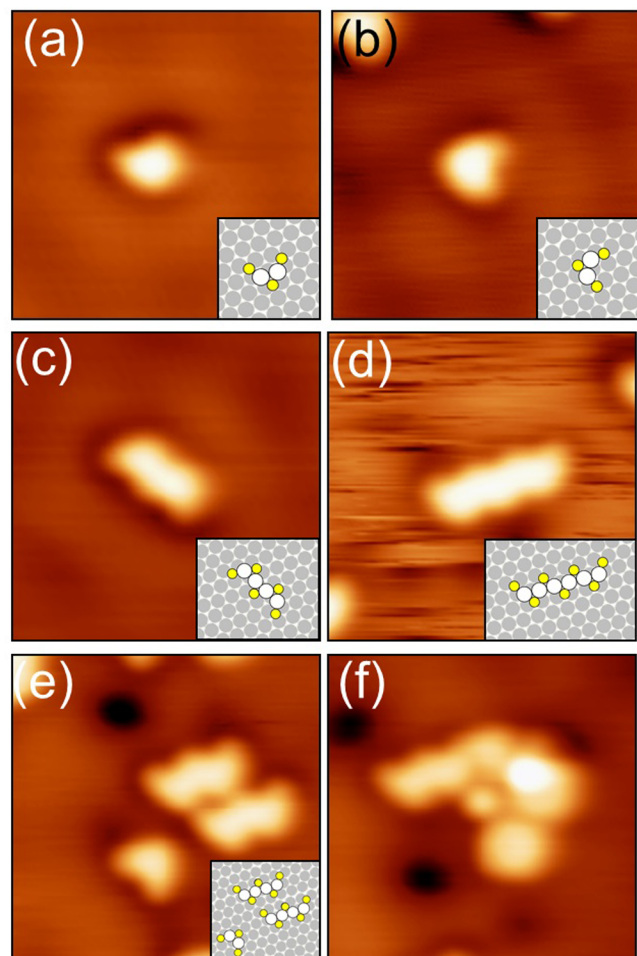


FIG. 3. Topographic STM images and proposed structures for Cu–S complexes on Cu(111) terraces. All images are $4.0 \times 4.0 \text{ nm}^2$. Insets show schematics of proposed configurations, with Cu atoms in the complex represented by white circles, S atoms by yellow, and Cu atoms in the substrate by grey. (a) and (b) 1-unit heart. (c) 2-unit linear chain of hearts. (d) 3-unit linear chain of hearts. (e) Two aligned 2-unit chains plus a heart. (f) Clump.

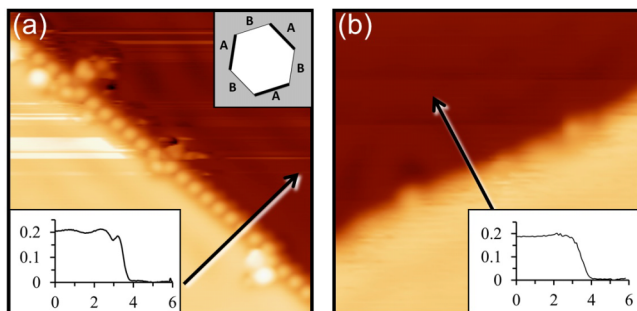


FIG. 4. Topographic STM images of A-type and B-type steps at $\theta_S < 0.004$ ML. Both images are $10 \times 10 \text{ nm}^2$. (a) A-type edge. Lower inset: Line profile across the step corresponding to the path indicated by the arrow. The x- and y-axes are in units of nm. Upper inset: Orientation of A- and B-steps in these experiments. The white hexagon represents an upper terrace. (b) B-type step with profile as described in (a).

the lowest θ_S in Fig. 2. Under these conditions, it is likely that the steps are sub-saturated. In Fig. 4(a), a step is smoothly decorated by a row of protrusions separated by 0.52 ± 0.02 nm, which we assign as S atoms at alternating sites along an A-step. This is very similar to our previous STM observation of S-decorated steps on a different surface, Ag(111)—cf. Fig. 3A of Ref. 30. In contrast, the step in Fig. 4(b), at 60° , is slightly irregular but not obviously decorated—and similar to the clean step in Fig. 1(d). We assign this as a nearly clean B-step.

The difference between A- and B-steps becomes more pronounced at higher θ_S , as shown in Figs. 5 and 6. Steps oriented close to the 3 A-directions are still smooth, while steps at other orientations display the jagged, triangular features first reported by Wahlström *et al.*²¹ We now examine the structures around steps more closely.

2. Structure around A-steps

The A-steps are characterized by a row of alternating S atoms at the edge, and a bright, linear feature that lies atop the upper terrace parallel to and near the step. Close inspection reveals that the linear feature resembles a terrace chain.

Quantitatively, the full-width at half-maximum (FWHM) of the bright linear feature is the same as the FWHM of the terrace chains, 0.56 ± 0.02 nm. It is significantly wider than single atoms of S which we have imaged on other surfaces [Au(100), Au(111), Au(110)] under the same conditions. For those cases, the atomic FWHM ranges from 0.29 to 0.38 nm. Furthermore, the bright feature has a distinctive zig-zag appearance in the differentiated STM images, and this also resembles the chains on the terraces. Examples and a schematic of the structure of the A-steps and the adjacent features are shown in Fig. 5. This model is supported by the DFT calculations presented in Sec. IV.

In addition, other chains are often found in the vicinity of A-steps, both on the upper and the lower terrace. Their lengths are skewed toward longer values than on terraces. Their locations and orientations, relative to the step edge, can vary. In short, the A-steps are rich in chains.

3. Structure around B-steps

Steps oriented close to the three B directions are lined with triangular features, which were first reported by Wahlström *et al.*²¹ High-magnification images are shown in Fig. 6, together with two schematic interpretations that are consistent with the DFT analysis developed in Sec. IV. Here, we summarize the distinctive features of the triangles, which are illustrated in Figs. 6(c) and 6(d).

(i) A slightly curved row of dots always defines the outer edge of a triangle, which is the edge facing the lower terrace—see green line in Fig. 6(c). These dots are spaced by $2a$, the measured value being 0.51 ± 0.02 nm ($N = 16$).

(ii) The inner edges of a triangle—the edges bordering the upper terrace as outlined in red in Fig. 6(c)—are also decorated by dots, separated by $2a$.

(iii) The features in the middle of the triangle depend on size. The smallest triangles are about $2.0\text{--}2.2$ nm on each interior edge, and they contain a single dot in the center. Together with the dots mentioned in (i) and (ii), this feature completes a local (2×2) -like pattern. The central dot is often slightly larger and higher than the dots at the edge. For larger

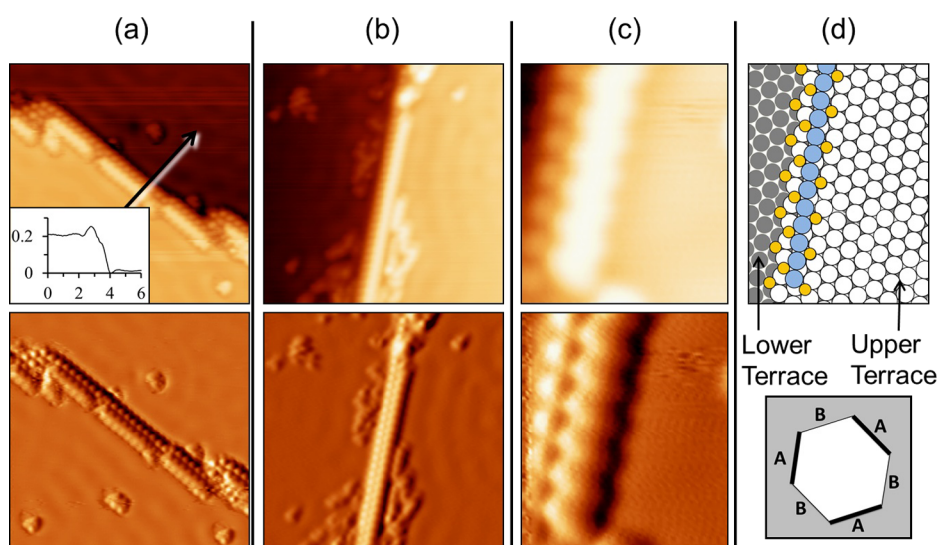


FIG. 5. STM images of A-steps with adsorbed sulfur, at high magnification. Each vertical pair shows the same data, but the top panel is topographic and the bottom is differentiated. (a) $\theta_S = 0.004$, $15 \times 15 \text{ nm}^2$. The inset shows the line profile across the step along the path shown by the arrow, with x- and y-axis units of nm. (b) $\theta_S = 0.016$, $15 \times 15 \text{ nm}^2$. (c) $\theta_S = 0.016$, $3.0 \times 3.5 \text{ nm}^2$. (d) Schematic model of (c), at approximately same scale. Grey circles represent Cu atoms at the level of the lower terrace, white circles are Cu atoms at the level of the upper terrace, and blue circles are Cu atoms adsorbed on top of the upper terrace. S atoms are small yellow circles.

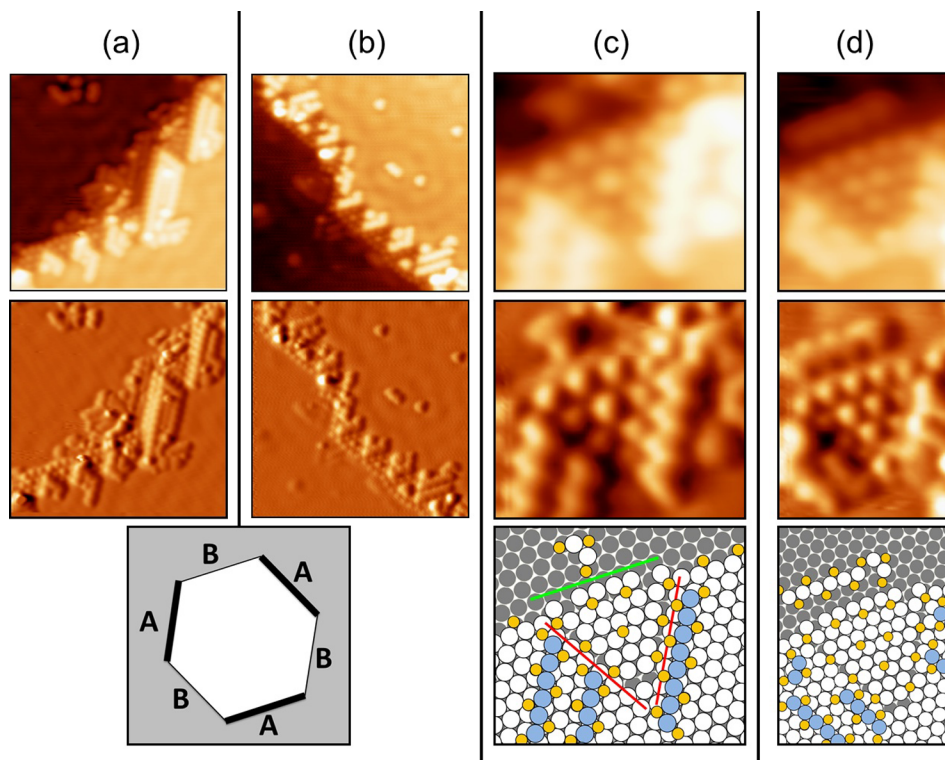


FIG. 6. STM images of B-step edges with adsorbed sulfur, at high magnification. Each vertical pair shows the same data, but the top image is topographic and the lower image is differentiated. (a) $\theta_S = 0.016$, $15 \times 15 \text{ nm}^2$. (b) $\theta_S = 0.016$, $15 \times 15 \text{ nm}^2$. (c) Small triangle. $\theta_S = 0.023$, $4.0 \times 3.5 \text{ nm}^2$. (d) Large triangle. $\theta_S = 0.023$, $3.5 \times 4.5 \text{ nm}^2$. In (c) and (d), the lowest panel is a schematic of a possible atomic structure, drawn to approximately the same scale as the STM images. The symbols and colors have the same meaning as in Fig. 5(d). Additionally, in (c), red lines show the triangle's inner edges, and the green line shows its outer edge.

triangles, with interior edges 2.9–3.0 nm, the interior region sometimes contains a larger (2×2)-like pattern, but more often, it is a diffuse elevated area with about the same apparent height as the upper terrace.

(iv) The inner edges of the triangle are aligned with A-steps.

(v) Immediately adjacent to the inner edges of the triangle, on the upper terrace, there are features with the height and appearance of chains. These are either oriented parallel to, or 60° from, the step edge.

Features (ii), (iv), and (v) above show that the orientations and features of the inner edges of the triangle bear a resemblance to the A-steps. Thus, it would be easy to conclude

that these are facets toward A-steps, as we did at an earlier stage in our analysis of this system.¹⁴ However, the situation is more complex, as will be discussed in Sec. IV.

In addition, B-steps commonly have a high density of miscellaneous extended chains in the near vicinity, both on the upper and lower terraces. This can be seen in Figs. 6(a) and 6(b). Again, this is similar to the A-steps. There is no obvious difference between A- and B-steps in the density of these miscellaneous chains.

IV. DFT ANALYSIS OF FEATURES AT AND NEAR STEP EDGES

A. Benchmark: Sulfur adsorbed on terraces

In the following analysis, a useful quantity is the chemical potential of S, μ_S , incorporated into a Cu_mS_n complex, $\mu_S(\text{Cu}_m\text{S}_n)$, which is defined as

$$\mu_S(\text{Cu}_m\text{S}_n) = [E(\text{Cu}_m\text{S}_n + \text{slab}) - E(\text{slab}) - m \mu_{\text{Cu}}]/n - E(\text{S}_{2,g})/2. \quad (1)$$

The chemical potential of Cu, μ_{Cu} , is the average energy of a Cu atom in the bulk. Note that μ_S reduces to the (average) adsorption energy of S for structures that do not incorporate additional Cu adatoms, i.e., for $m = 0$. This quantity, μ_S , allows us to assess the relative stability of various complexes in the presence of excess S beyond that required to saturate step edges.

Figure 7 shows $\mu_S(S)$ as a function of θ_S on the Cu(111) terrace, calculated from DFT. As supercell size decreases, θ_S increases. Three sets of calculations, based on 3 types of supercells, are represented. Green symbols show

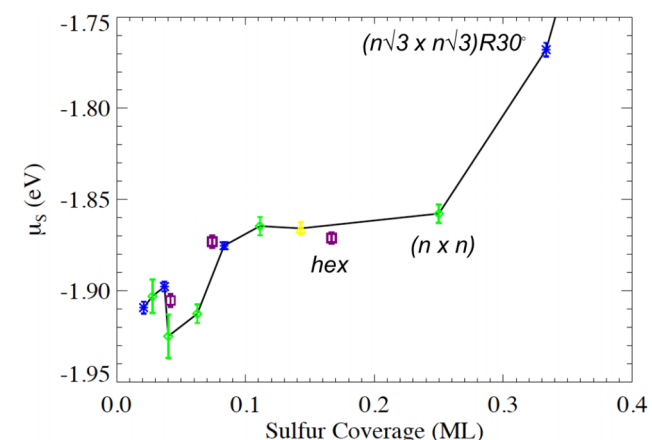


FIG. 7. Chemical potential (adsorption energy) of adsorbed S vs. θ_S , calculated from DFT. Green symbols show $(n \times n)$ supercells, blue show $(n\sqrt{3} \times n\sqrt{3})R30^\circ$ supercells, yellow shows a $(\sqrt{7} \times \sqrt{7})R19^\circ$, and purple show honeycomb (hexagonal) supercells in which there are 2 adatoms per unit cell, both occupying fcc sites.

TABLE I. Chemical potential (adsorption energy, in eV) of a single row of adsorbed S on an A-step and a B-step with different supercells and island widths. B1 is a structure with S on the upper edge of a B-step. Configurations for the (2×8) are shown in Fig. 8.

$\mu_S(S)$	2×4	2×6	2×8	2×10
A-step	-2.27(1)	-2.227(6)	-2.240(4)	
B-step	-2.20(1)	-2.15(2)	-2.13(1)	-2.14(1)
B1	-2.16(2)	-2.08(1)	-2.11(1)	-2.11(1)

($n \times n$) supercells, blue show ($n\sqrt{3} \times n\sqrt{3}$)R30° supercells, yellow shows a ($\sqrt{7} \times \sqrt{7}$)R19°, and purple show honeycomb (hexagonal) supercells in which there are 2 adatoms per unit cell, both occupying fcc sites. At low θ_S , $\mu_S(S)$ depends sensitively on the nature of the supercell. The ($n \times n$) calculations show high scatter and large error bars at low coverage, so are regarded as least reliable. The points below 0.070 ML cluster around -1.90 to -1.92 eV, which leads to our choice of -1.91 eV as the low-coverage limit for $\mu_S(S)$.

B. Extended structures at step edges

For extended structures that run along the step edges, we carry out DFT calculations using ($2 \times 2n$) supercells, since most of the structures of interest are assumed to have periodicity of $2a$ along the step edge. In practice, we choose the primitive cell for this set of calculations as a rectangular ($1 \times \sqrt{3}$), because k -points' grids for asymmetrical supercells are easier to implement with a rectangular lattice than with a triangular lattice. The most important DFT results for the step edges are shown in this section; other related DFT results are given in the Appendix. For purposes of comparison between STM data and DFT results, we consider that the step edges at $\theta_S \geq 0.004$ are locally saturated, since the features in the immediate vicinity of the steps (e.g., the chain atop the A-step) do not change in this coverage range.

We first consider configurations with a single row of S atoms at a step edge (represented as the edge of a 4 Cu atom wide strip in the first layer). Table I shows the results for supercells of size ($2 \times 2n$), where we put a ($2 \times n$) island of Cu adatoms on top of the slab. Figure 8 illustrates the (2×8) supercell configurations.

In Table I, note first that all values of $\mu_S(S)$ are lower than the -1.91 eV for S on fcc sites, so adsorption of S at steps is more favorable than at terraces. Comparing A- and B-steps,

$\mu_S(S)$ is always more negative at the A-step than at the B-step, consistent with the interpretation of Fig. 4. Finally, comparing upper and lower step edges, $\mu_S(S)$ is consistently lower when S adsorbs at the lower step edge than at the upper step edge, where the latter is represented by configuration B1.

We next consider 2 rows of S attaching to a step edge (now represented as the edge of a 5 atom wide strip in the first layer). Some configurations are shown in Fig. 9. For the A-step ((a)-(c)), we find that the most stable configuration has the Cu atoms in the outermost row of the step shifting and forming a pseudo (100) surface, which can be viewed as an extended step edge reconstruction [see Fig. 9(c)]. For a B-step ((d) and (e)), the most stable configuration has the upper row of S atoms adsorbed on the unreconstructed step edge at fcc sites [see Fig. 9(d)].

Can more S aggregate at an A-step? Figures 10(a)-10(c) show 3 configurations with 3 rows of S close to an A-step. Figure 10(a) does not have any additional Cu atoms beyond the 5 atom wide strip in the first layer also shown in Fig. 9, but the 2 outermost rows of Cu reconstruct forming a pseudo (100) surface. Figures 10(b) and 10(c) are very similar. Both have 2 extra second-layer Cu atoms in each supercell (in addition to the 10 Cu atoms per unit cell that form the 5-atom wide strip). Together with the 2 S atoms on top of the island, the extra Cu atoms form a one-atom row of Cu with S on either side, i.e., a zigzag S–Cu–S chain. The difference between Figs. 10(b) and 10(c) is the distance between the chain and the step edge, with (c) being closer. With a 5-atom wide island, we find the configuration in Fig. 10(c) to be the most stable, involving 3 rows of S around an A-step. (It is interesting to note that Cu atoms in the chain actually are closer to bridge sites than to either of the two 3fh (fcc or hcp) sites.) This structure is entirely consistent with the interpretation of the STM images of the A-step at $\theta_S \geq 0.004$ given in Sec. III [Fig. 5], which are based largely on empirical observation. Thus, the configuration in Fig. 10(c) is confirmed experimentally.

Based on DFT, there is a possibility that the A-step in the STM image in Fig. 4(a) is a 2-row decoration of S, rather than the 1-row interpretation given elsewhere in this paper. In support of this, the circular shape of the dots in the STM data is much better-matched in the simulated image for the double-row model [Fig. 9(c)] than the 1-row model [Fig. 8(a)]. However, the dot is predicted to be higher (brighter) than the Cu terrace in the double-row model, whereas in experiment,

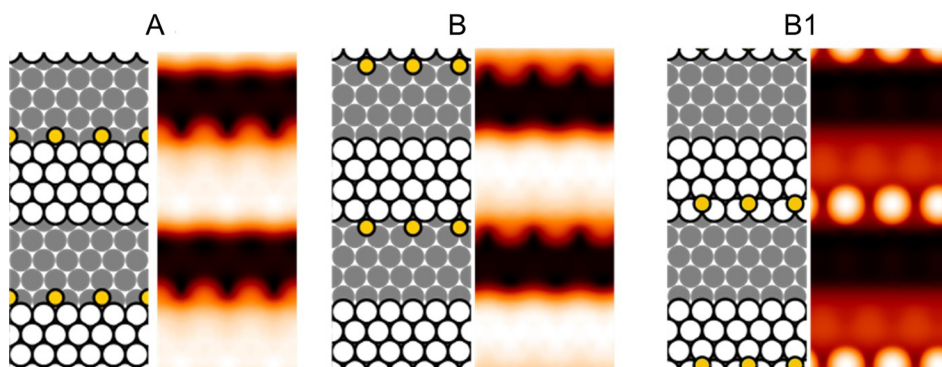


FIG. 8. Optimized DFT configurations and simulated STM images of a single-row of S attaching to the A- or B-step, for a (2×8) supercell. Chemical potentials are given in Table I. Symbols and colors in the configurations have the same meaning as in Fig. 5(d).

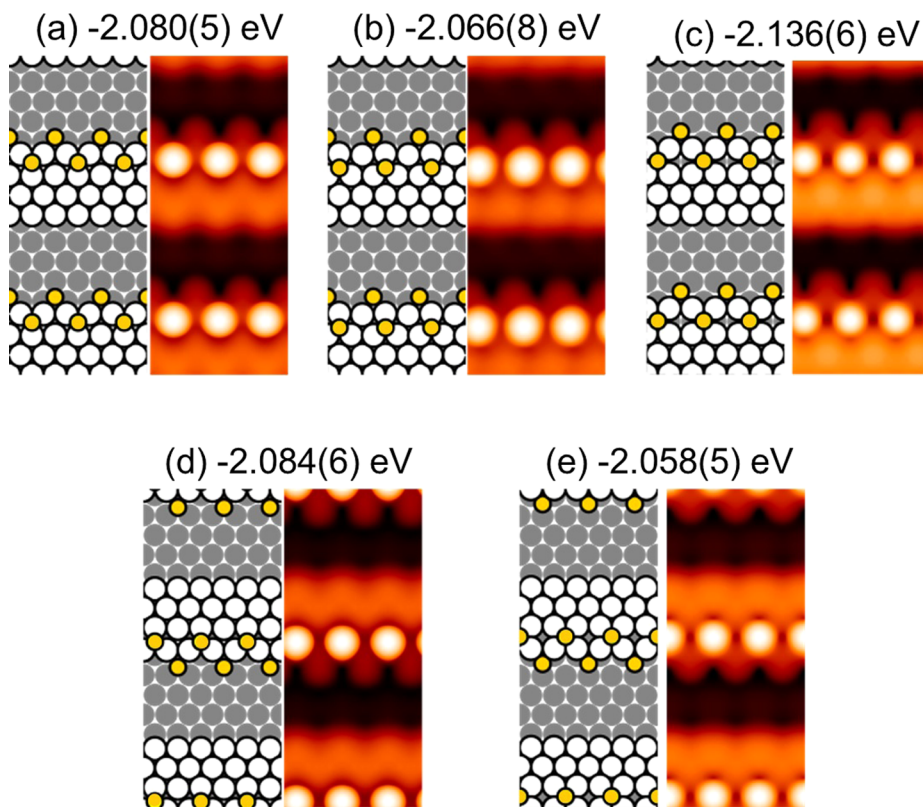


FIG. 9. Optimized DFT configurations, simulated STM images, and chemical potentials of S for various 2-row configurations of S at A-steps ((a)-(c)) and at B-steps ((d) and (e)), for (2×8) supercells. The chemical potential here is the average adsorption energy of S in the two different environments. Symbols and colors in the configurations have the same meaning as in Fig. 5(d).

the dot is always below the level of the upper terrace [see line profile in Fig. 4(a)]. At present, we cannot decide between these two possibilities. In principle, they are not mutually exclusive, since there should be a transition from 1- to 2- to

3-row S structures at the A-steps as θ_S increases. In either case, the A-step is sub-saturated.

Turning now to the B-step, Figs. 10(d)-10(f) show 3 configurations with 3 rows of S. In Fig. 10(d), the upper terrace

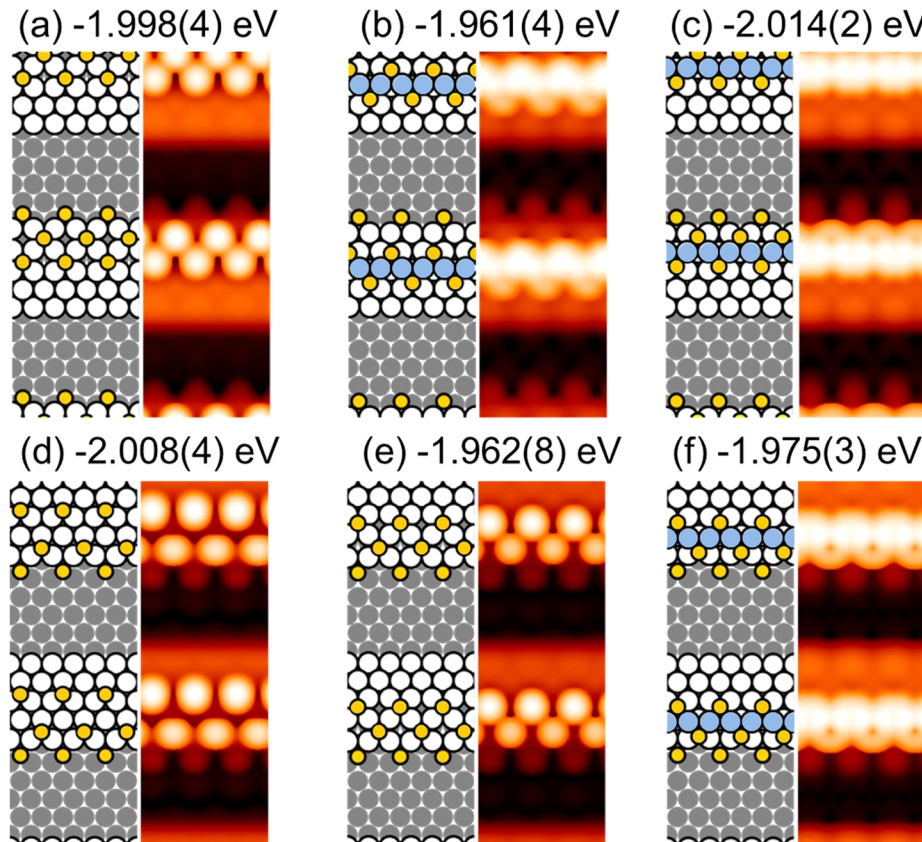


FIG. 10. Optimized DFT configurations, simulated STM images, and calculated chemical potentials of S for three rows of S near the A-steps ((a)-(c)) and near the B-steps ((d)-(f)). In (b), (c), and (f), the blue circles represent an additional row of Cu on the upper terrace. This, combined with two of the three S rows, forms a S–Cu–S chain on the upper terrace. Symbols and colors in the configurations have the same meaning as in Fig. 5(d).

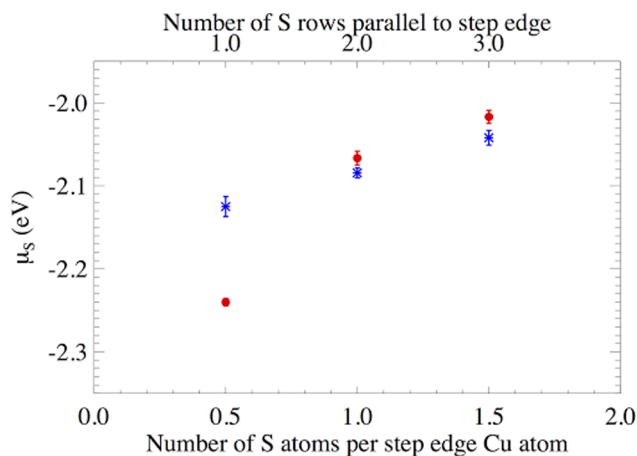


FIG. 11. Chemical potential of S decorating A-type (red) and B-type (blue) steps with increasing coverage of sulfur at the step edge, calculated from DFT.

S atoms are all on fcc sites. Figure 10(e) has the outmost row of Cu shifted to form a pseudo (100) surface. Figure 10(f) has 2 additional Cu atoms per supercell, forming a zigzag S–Cu–S chain. However, as we show in Sec. IV C, the B-step is prone to massive rearrangement at high local θ_S and extended structures such as these are not expected to exist.

Figure 11 and Table II summarize DFT results from this section, showing $\mu_S(S)$ as a function of S coverage at the step edge. Based on the energetics, at an A-step, one expects a transition from 1- to 2- to 3-row S structures with increasing θ_S . The same expectation would in principle apply to the B-step, except that the B-step is unstable against massive distortion with increasing θ_S , as will be discussed in Sec. IV C. In all cases, $\mu_S(S)$ is lower at a step than on a terrace, for which $\mu_S(S) = -1.91$ eV. This is consistent with the experimental observations of heavy step decoration [Figs. 2, 5, and 6] at all except the very lowest θ_S , where the steps are sub-saturated [i.e., in Fig. 4].

C. Triangular features on B-steps

When θ_S at a B-step increases above a single row, DFT calculations show that distortions of the simple extended structures studied in Sec. IV B can lower the energy. Figure 12 provides two examples where the starting point is a partial (a) or complete (b) double extended row of S atoms. Figure 12(a) shows that for a pair of S atoms at the upper step edge separated by $2a$, the energy of the system is reduced if three Cu atoms between the S pairs move down from original fcc sites to nearby hcp sites, thus forming two local 4fh sites [denoted by red circles in Fig. 12(a)] where the pair of S atoms can reside. The lower panel shows a similar distortion at higher

TABLE II. Chemical potentials of S, in eV, for most favorable configurations of 1-, 2-, and 3-row S at A- and B-steps of Cu(111).

	1-row S	2-row S	3-row S
A-step	-2.24	-2.14	-2.01 (With chain)
B-step	-2.11	-2.08	n/a

θ_S , but involving more Cu atoms and producing local 4fh sites that are further apart. Interestingly, these distortions produce interlocking wedge-shaped regions in the step edge, which can be described as areas where the Cu atoms remain in their original fcc sites, alternating with complementary areas where all Cu atoms are shifted away from original fcc sites.

It is natural to extend the picture to larger distortions so that more 4fh sites are formed. Figure 13(a) shows the structure obtained from DFT using a 3-layer slab with a (9×9) supercell (with single k-point). A triangular array of 26 Cu atoms is shifted from fcc sites to hcp sites, forming a domain boundary of 4fh sites. (Not all Cu atoms in the triangle are in hcp sites; 4 Cu atoms at the bottom are in fcc sites.) Altogether, they can accommodate 8 S adatoms on 4fh sites. A 9th S atom is adsorbed on a 3fh site in the center.

The accompanying STM simulation in Fig. 13(b) shows a triangular area with 8 spots at almost the same height as the Cu island. The 9th spot in the center is slightly brighter. [Terms used to describe the STM images are defined in Fig. 13(c).] This simulation is in excellent agreement with the measured STM images of small triangles at B-steps, which can be confirmed by comparing the following aspects of Figs. 13(b) and 13(d): (i) a distinctive, slightly curved row of 4 dots at the outer edge of the triangle (S atoms in 4fh sites); (ii) 4 additional dots along the inner edges of the triangle (S atoms in 4fh sites); (iii) a central dot slightly larger and higher than the dots at the edges (S atom in 3fh site); (iv) arrangement of the 9 dots together in a (2×2) -like pattern; and (v) interior edges of the triangles parallel to A-steps. We therefore assign small triangles in the B-steps to this structure.

We have extended the calculation to an even larger configuration based on a (12×12) supercell, $L = 3$, and a single k-point grid. The energy-optimized configuration is shown in Fig. 14(a) and its corresponding STM simulation in Fig. 14(b). This time there are 5 dots along the curved outer edge and 6 dots along the inner edges of the triangle, all corresponding to S atoms in 4fh sites. In addition, the model has 3 central S atoms in 3fh sites. Altogether, in the model, there are 14 S atoms arranged in a (2×2) -like array within the triangle. All of these features, including the internal (2×2) -like lattice with 3 central dots slightly brighter and larger than the others, are observed experimentally, for instance, in the topographic image of Fig. 6(d).

However, the experimental image in Fig. 14(c) shows a heart-shaped feature near the center of the triangle, rather than a (2×2) -like array. To mimic this feature, 2 additional Cu adatoms are inserted [blue circles in Fig. 14(a)] in the space between 3 S atoms, above the layer of displaced Cu atoms. This results in a Cu_2S_3 complex that, in turn, produces a heart shape in the simulated image of Fig. 14(b). This gives a clue as to how and why the interiors of the large triangles are often elevated, or “filled in” in the experimental images: the interiors become populated with second-layer Cu adatoms in addition to S adatoms.

V. DISCUSSION

Our experimental results, interpretation of which is supported and enhanced by DFT analysis, reveal a variety

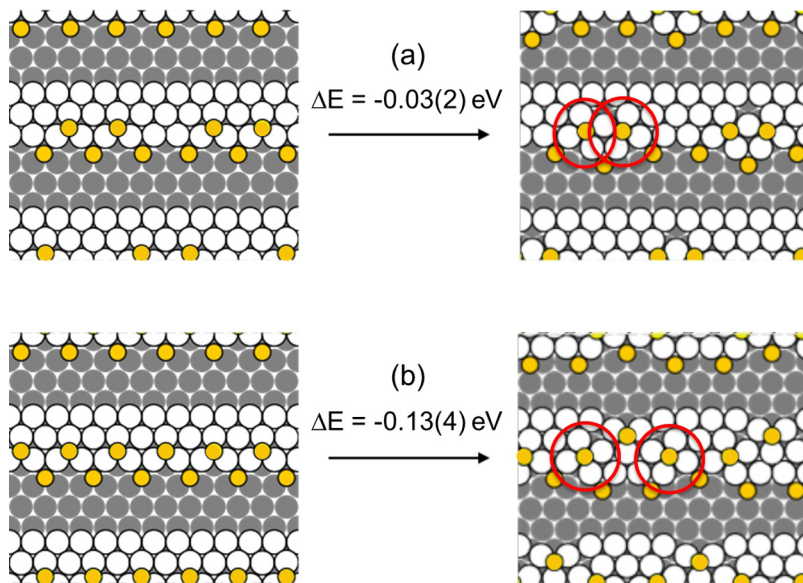


FIG. 12. Distortion induced by adsorption of S on B-steps. Symbols and colors in these DFT-optimized configurations have the same meaning as in Fig. 5(d).

of S-induced structures at step edges, in addition to those on terraces. Two of these are particularly intricate and unanticipated.

The first is the 3-row S structure at the A-steps, shown in Figs. 5(d) and 10(c). One row of S is at the lower step edge, and two S rows exist as part of a zig-zag S–Cu–S chain which involves an extra row of Cu in the second layer at the upper step edge. Cu adatoms in the chain do not occupy normal fcc sites, but they do provide high-coordination sites for S adatoms on both sides. The result is that S adatoms in all 3 S rows occupy p4fh sites.

The adsorption of Cu adatoms in near-bridge adsorption sites in the upper chain, resulting from global energy optimization in DFT, suggests that the energy penalty for moving Cu away from the natural 3fh fcc adsorption site is offset by the energy gain from Cu–S bonding. This is consistent with the conclusion from our previous study of Cu_2S_3 on terraces.¹⁴ The dominant feature in those complexes is strong Cu–S bonding, both within the complex (which favors linear S–Cu–S units) and between S atoms in the complex and Cu atoms in the substrate (which favors high-coordination adsorption sites for S). Cu–Cu bonding between the complex and the substrate is

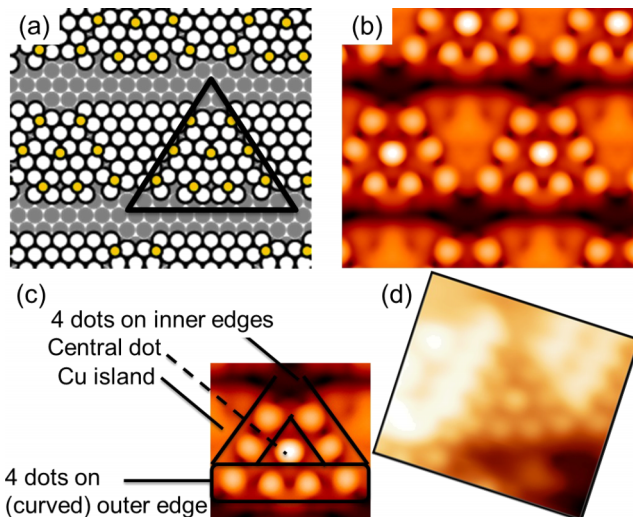


FIG. 13. Model for the small triangular features along a B-step. (a) Optimized configuration from DFT. The majority of the Cu adatoms inside the outlined triangle are on heptagonal close-packed (hept) sites, forming 8 p4fh sites, each occupied by a S atom. One extra S atom in the middle of the triangle is on a 3fh site. Symbols and colors have the same meaning as in Fig. 5(d). (b) Simulated STM image. (c) Schematic, clarifying terms used in the discussion of the STM images. (d) Actual topographic STM image of a small triangle [the same as Fig. 6(c)], $4.0 \times 3.5 \text{ nm}^2$. The experimental image is manipulated to be about the same size and orientation as the triangle in the simulated image.

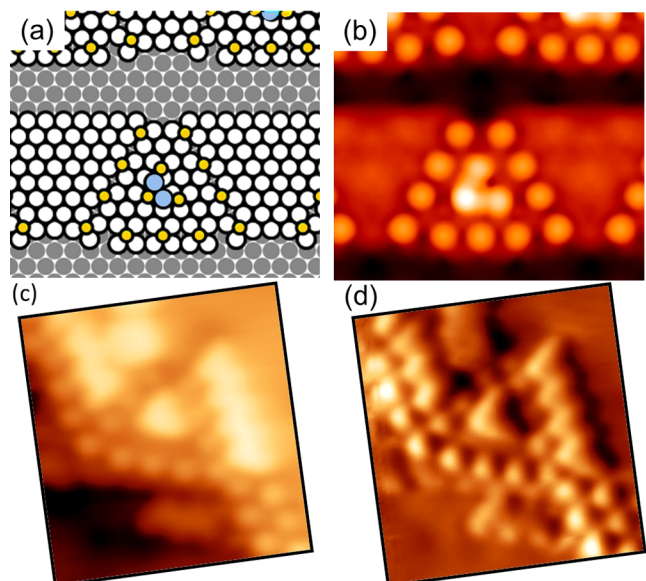


FIG. 14. Model for the large triangular features along a B-step. In this particular case, a Cu_2S_3 complex resides in the middle of the triangle. (a) Optimized configuration. Cu atoms in the Cu_2S_3 complex are in blue (on-line). (b) Simulated STM image. (c) and (d) Actual topographic and differentiated STM image of a large triangle (similar to Fig. 6(d), but a different triangle), $4.0 \times 4.5 \text{ nm}^2$. The experimental image is manipulated to be the same size and orientation as a triangle in the simulated image.

of lesser importance, so the favored adsorption site of Cu is sacrificed.

The second is the triangle motif at B-steps, shown in Figs. 6(c), 6(d), 13(a), and 14(a). The triangles are reconstructions in which a group of Cu atoms moves out of their original fcc sites toward the lower terrace, forming a less-dense network and providing 4fh sites for most of the S adatoms. When a triangle is large enough, its inner area can fill in with additional, upper-level Cu atoms, but the interior edges are always preserved. At the upper level of interior edges, zig-zag S–Cu–S chains can usually be found that are very similar to the A-step upper-level chains. Excellent agreement is obtained between the DFT-based STM images of this complex structure and the experimental STM images. In particular, two distinctive details are reproduced: the slight curvature in the row of dots (S atoms in 4fh sites) at the external edge of the triangle and the enhanced brightness of the dots (S atoms in 3fh sites) in the center of the triangle relative to those at the edges.

Thus, both structures can be understood as step reconstructions that create (p)4fh sites for S adsorption, at the expense of Cu registry, while also incorporating features (chains) that reflect the importance of the S–Cu–S subunit.

The features in our experiments are completely static at 5 K. Our data do not provide information about thermal stability. However, Wahlström *et al.* observed well-defined triangles, with edge lengths comparable to those in our experiments, at 300 K—cf. Fig. 1 of Ref. 20—along steps aligned with 3 of the close-packed directions, i.e., B-steps. They reported that the triangles changed in both size and position, although this was sensitive to tunneling conditions and hence likely to have been tip-assisted. It is not clear whether chains on upper levels (or elsewhere) were present, but at least, one can conclude from their data that the main bodies of the triangles on B-steps are stable at 300 K. Oriented at 180°, another step was imaged that would necessarily have been an A-step. It was frizzy and much different than our A-steps at 5 K. The frizziness reflects atomic motion on the time-scale of scanning and has been well-documented for clean surfaces of Cu(111).³¹ Even though the step structure is dynamic, it is possible that S continues to influence motion along the A-steps, as we demonstrated to be true for sulfur on Ag(111).³² But the main conclusion derived from this comparison is that the static 3-row S structure of the A-step is not retained at 300 K.

We noted in Sec. III that “miscellaneous” chains are commonly found around step edges. They are more abundant around steps than on terraces and also longer on average. This implies that step edges participate in generating the terrace complexes. One possible mechanism involves the triangles at B-steps. The outer edge of the triangle is bounded by Cu atoms [cf. Fig. 13(a) or 14(a)]. Addition of S atoms at the outer edge could destabilize the structure, whereupon a Cu–S chain parallel to the step edge could peel off and diffuse out onto the terrace, and the triangle would adjust accordingly. This hypothesis is consistent with the fact that a separate chain is sometimes observed adjacent and parallel to the outer edge of a triangle. A clear example is Fig. 6(d). Another possible way of generating chains on terraces could be movement of

chains at the upper step edges away from the steps. This finds support in the observation that there are sometimes two or three chains decorating upper A-steps or upper edges of triangles on B-steps, as if chains are generated successively at these upper edges. There may be other mechanisms as well by which chains/hearts on terraces are generated, depending on temperature, θ_S , and step density. The relationship between the steps and the complexes on terraces is a topic of continuing investigation.

Finally, we can compare this study of S/Cu(111) with a prior study of S/Ag(111) under identical conditions.³⁰ At very low θ_S and at 5 K, S–Ag complexes existed on Ag(111) terraces, both in the form of individual units and concatenated chains. The steps were modified by S adsorption. Some evidence suggested that the steps participated in forming the complexes. In these respects, the observations for the two close-packed coinage metal surfaces are analogous. However, the structures proposed for the terrace complexes on Ag(111) were quite different, and triangles were not observed on S/Ag(111) step edges.³⁰

VI. CONCLUSIONS

We have identified the reconstructions of A- and B-steps on Cu(111) that exist at low θ_S and low T. In both cases, S can adsorb at (p)4fh sites. This is different than the structural motifs of Cu–S moieties on terraces at these coverages, which may be due to the higher local θ_S at the step edges than at the terraces. Based on comparison with other published work, one of these reconstructions is stable to (at least) room temperature.²⁰ A mechanism is postulated by which the reconstructed steps could produce Cu–S chains on terraces.

ACKNOWLEDGMENTS

The experimental component of this work was supported by three sources. From the U.S., it was supported by NSF Grant Nos. CHE-1111500 and CHE-1507223. From Japan, support was provided by a Grant-in-Aid for Scientific Research on Priority Areas “Electron Transport Through a Linked Molecule in Nano-scale” and a Grant-in-Aid for Scientific Research(S) “Single Molecule Spectroscopy using Probe Microscope” from the Ministry of Education, Culture, Sports, Science, and Technology (MEXT). The theoretical component of this work was supported by the Division of Chemical Sciences, Basic Energy Sciences, U.S. Department of Energy (USDOE), and it utilized resources of the National Energy Research Scientific Computing Center, which is supported by the Office of Science of the U.S. Department of Energy (Contract No. DE-AC02-05CH11231). We thank Kan Ueji and Hiroshi Imada for assistance with the experiments.

APPENDIX: ADDITIONAL STRUCTURES STUDIED WITH DFT

Other structures of interest that have been studied with DFT, but not discussed in the main text, are included in this supplementary material.³³

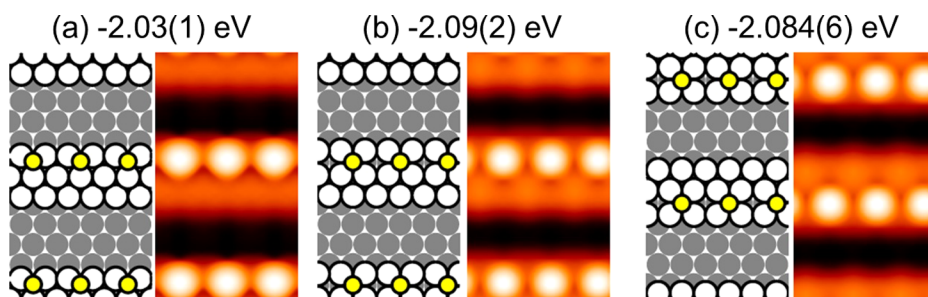


FIG. 15. Structures, simulated STM images, and chemical potentials for various 1-row configurations of S at step edges. The A-step is the upper edge of the Cu island, and the B-step is the lower edge.

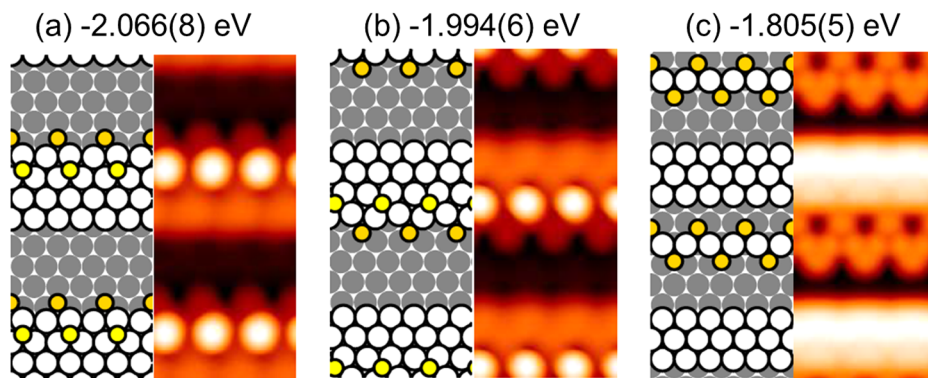


FIG. 16. Structures, simulated STM images, and chemical potentials for various 2-row configurations of S at step edges. The A-step is the upper edge of the Cu island, and the B-step is the lower edge.

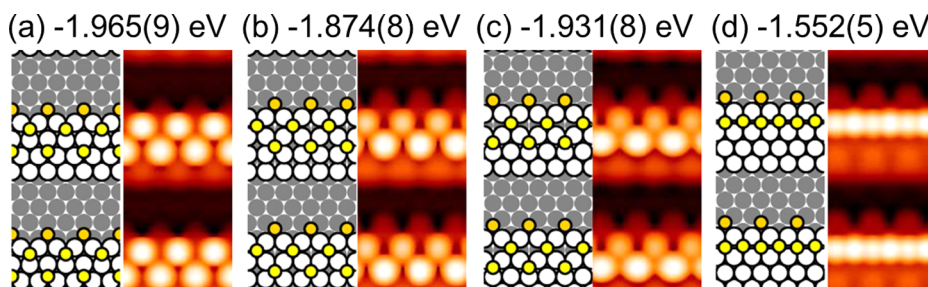


FIG. 17. Additional 3-row S configurations. The A-step is the upper edge of the Cu island, and the B-step is the lower edge.

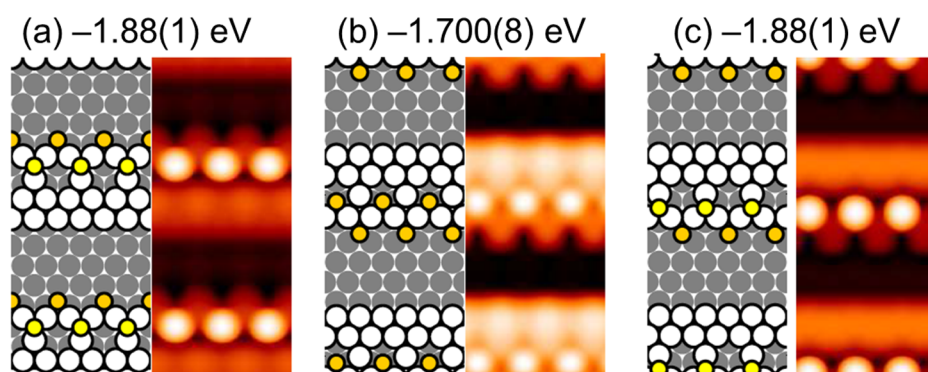
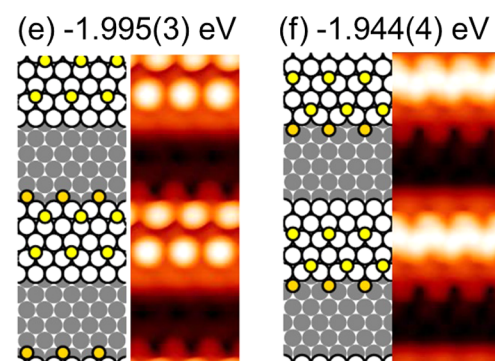


FIG. 18. Similar to Fig. 16, but with vacancies introduced near the step edge. The A-step is the upper edge of the Cu island, and the B-step is the lower edge.

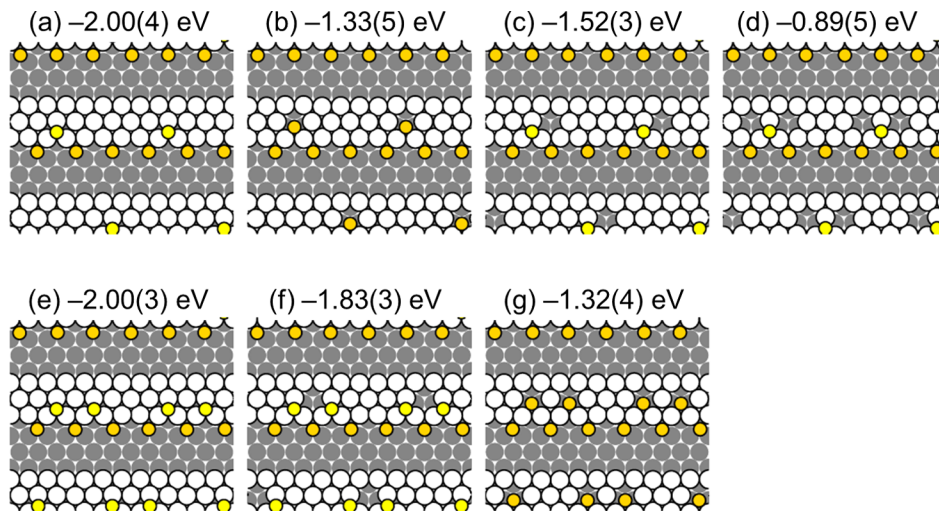


FIG. 19. Comparison of chemical potential of 2-row S configurations with and without vacancies. Note that for this figure, μ_S quoted is only for upper edge S.

1. Additional 1-, 2-, and 3-row configurations

Figure 15 shows some additional examples of 1-row configurations of S at step edges. Figure 15(a) has the S at a fcc site at the upper A-step edge, and (b) has the leading edge Cu atom shifted outward to an hcp site, forming 4fh sites occupied by S, while (c) has a similar arrangement as (b) but at the B-step.

Figure 16 shows additional 2-row configurations. Figure 16(a) is similar to the 2-row structure shown in the main text at an A-step (Fig. 9), but with the S at the upper step edge at a fcc site, rather than a hcp site, so it is not exactly between the two lower edge S atoms. Figure 16(b) is analogous to (a) but at the B-step. Here, the Cu atoms shift slightly away from fcc sites, creating low-symmetry sites for S. Figure 16(c) starts from a reconstructed step edge similar to (b), but with the outermost Cu further away from the step. The optimized structure has the outermost row of Cu moving even further away from the step edge and forming a separated Cu–S zigzag chain.

Figure 17 shows additional 3-row S configurations at step edges. Figure 17(a) has the second row S at hcp sites, and the third row S at fcc sites, at an A-step. Figures 17(b) and 17(c) involve A-step edge reconstruction and are subtly different from the reconstructed A-step edge mentioned in the text (Fig. 10). Figure 17(b) has the second and the fourth row shifted, while (c) has only the first row shifted. In comparison, the reconstruction mentioned in the main text has the second row shifted. (d) has the third row pushed towards the second row, thus forming an overly saturated row. (e) is similar to (a), but with third row shifted to fcc sites further away from the step edge. Note that it is slightly more stable than (a), indicating

there is no driving force for a third row of S to move very close to step edges in these arrangements. Finally, (f) is similar to (e) but on a B-step.

2. Step structures incorporating Cu vacancies

Next, we focus on possibilities that a step can be stabilized by the introduction of vacancies. Figure 18 shows some examples with vacancies near the step edge and 2-row S decoration. In all calculations involving step edges, the clean slab has an existing island. The chemical potential thus calculated does not include the energy cost of forming the step edges but does include the energy cost of forming the vacancies. As shown in these calculations, it is easier to extract a Cu atom not bonded with any S, than to extract a Cu atom bonded with a S, and then let the S fall down into the vacancy. Overall, for the configurations tested, the chemical potentials indicate that vacancies do not stabilize steps.

One can calculate the formation energy of the vacancy using $E_f = n(\mu_S^v - \mu_S^0)$, where $n = 2$ is the number of S atoms, and $\mu_S^{v(0)}$ is the chemical potential of S with (without) the vacancy. For Figs. 18(a) and 18(c), $E_f = 0.33$ and 0.31 eV, respectively. This is much lower than the formation energy of a vacancy on a clean Cu(111) surface, estimated to be 0.78 eV from DFT.²⁷

We also consider some partial 2-row S configurations with vacancies at B steps and compare them with similar configurations without any vacancy. This is shown in Fig. 19. Based on the chemical potentials, we conclude that vacancies do not stabilize steps in this range of configurations, either.

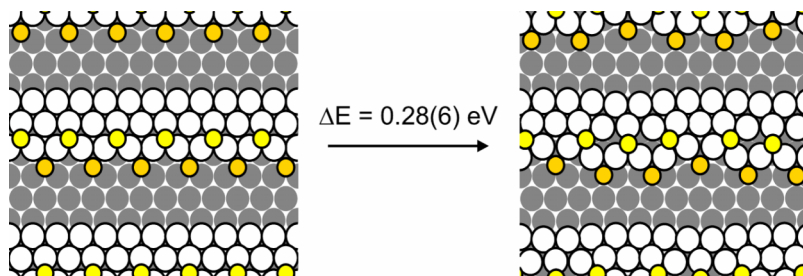


FIG. 20. Change in energy by peeling out a row of Cu together with S on a S-decorated B-step.

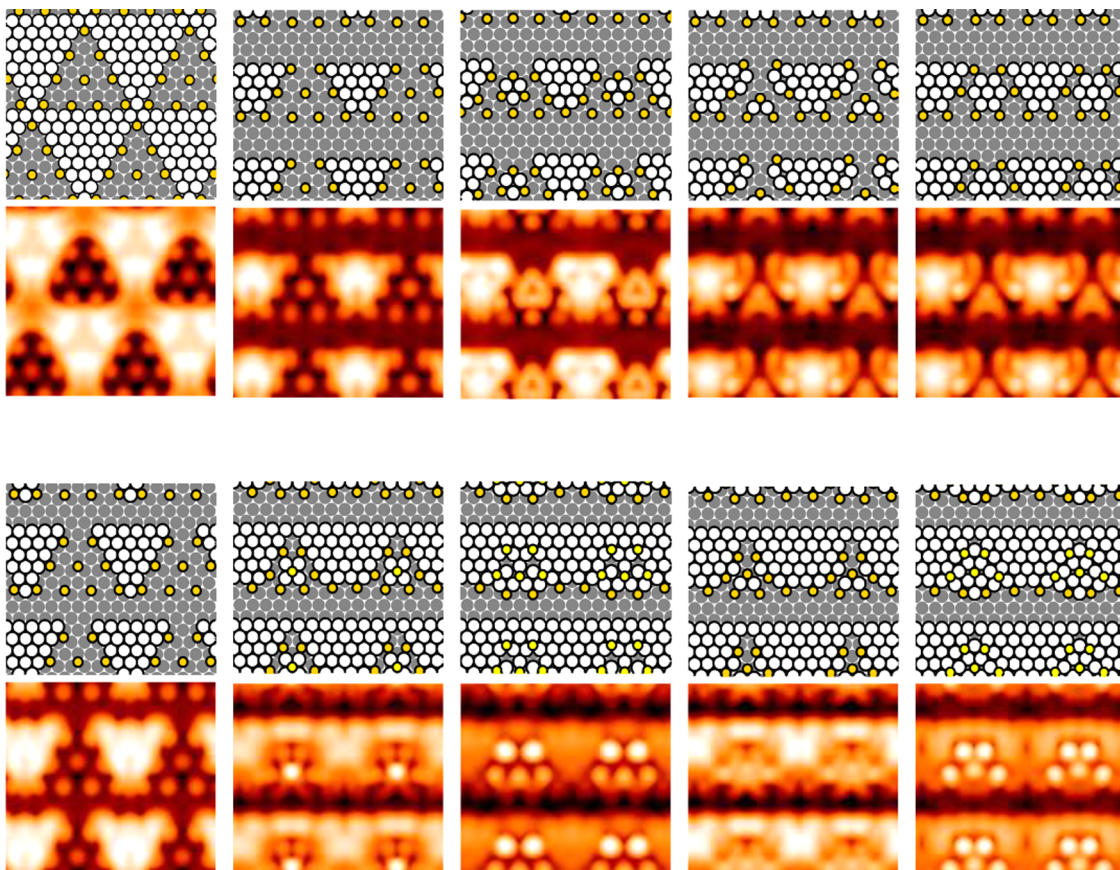


FIG. 21. Selected structures and their simulated STM images for triangular features calculated in a (8×8) supercell.

The configuration with lowest formation energy for a vacancy is in Fig. 19(f), where $E_f = 0.33$ eV.

3. Alternative formation mechanism for Cu–S chains

Figure 20 shows the change in energy by moving two Cu atoms at the B-step away from the step in an attempt to peel off a Cu–S chain from the S decorated B-step. The positive sign of ΔE shows that the configuration on the right is only metastable.

4. Other configurations for the B-type triangular structure

Figure 21 shows samples of other triangular structures that were investigated as part of the effort to interpret the triangular features seen at B-steps in experimental STM images. Most of them are not carried out to sufficient length to have reliable energetics. Based on a combination of approximate energetics and agreement with experimental STM images, we discard these structures in favor of the structure presented in the main text.

¹B. L. M. Hendriksen, M. D. Ackermann, R. van Rijn, D. Stoltz, I. Popa, O. Balmes, A. Resta, D. Wermeille, R. Felici, S. Ferrer, and J. W. M. Frenken, “The role of steps in surface catalysis and reaction oscillations,” *Nat. Chem.* **2**(9), 730–734 (2010).

²S.-L. Chang and P. A. Thiel, “Atomic-scale mechanisms of metal-on-metal film growth,” *CRC Crit. Rev. Surf. Chem.* **3**, 239–296 (1994).

³L. Li, L. Luo, J. Ciston, W. A. Saidi, E. A. Stach, J. C. Yang, and G. Zhou, “Surface-step-induced oscillatory oxide growth,” *Phys. Rev. Lett.* **113**, 136104 (2014).

⁴C.-Y. Ruan, I. Stensgaard, F. Besenbacher, and E. Laegsgaard, “A scanning tunneling microscopy study of the interaction of S with the Cu(111) surface,” *Ultramicroscopy* **42-44**, 498–504 (1992).

⁵P. A. Thiel, M. Shen, D.-J. Liu, and J. W. Evans, “Critical review: Adsorbate-enhanced transport of metals on metal surfaces: Oxygen and sulfur on coinage metals,” *J. Vac. Sci. Technol., A* **28**(6), 1285–1298 (2010).

⁶P. Maksymovych, O. Voznyy, D. B. Dougherty, D. C. Sorescu, and J. T. Yates, Jr., “Gold adatom as a key structural component in self-assembled monolayers of organosulfur molecules on Au(111),” *Prog. Surf. Sci.* **85** (5-8), 206–240 (2010).

⁷L. Bartels, “Tailoring molecular layers at metal surfaces,” *Nat. Chem.* **2**(2), 87–95 (2010).

⁸M. Garvey, J. Kestell, R. Abuflaha, D. W. Bennett, G. Henkelman, and W. T. Tysoe, “Understanding and controlling the 1,4-phenylene diisocyanide-gold oligomer formation pathways,” *J. Phys. Chem. C* **118**(36), 20899–20907 (2014).

⁹K. Diller, F. Klappenberger, F. Allegretti, A. C. Papageorgiou, S. Fischer, A. Wiengarten, S. Joshi, K. Seufert, D. Ecija, W. Auwarter, and J. V. Barth, “Investigating the molecule-substrate interaction of prototypic tetrapyrrole compounds: Adsorption and self-metalation of porphine on Cu(111),” *J. Chem. Phys.* **138**(15), 154710 (2013).

¹⁰P. J. Feibelman, “Formation and diffusion of S-decorated Cu clusters on Cu(111),” *Phys. Rev. Lett.* **85**, 606–609 (2000).

¹¹W. L. Ling, N. C. Bartelt, K. Pohl, J. de la Figuera, R. Q. Hwang, and K. F. McCarty, “Enhanced self-diffusion on Cu(111) by trace amounts of S: Chemical-reaction-limited kinetics,” *Phys. Rev. Lett.* **93**(16), 166101 (2004).

¹²M. Foss, R. Feidenhans'l, M. Nielsen, E. Findeisen, T. Buslaps, R. L. Johnson, and F. Besenbacher, “Sulfur induced Cu₄ tetramers on Cu (111),” *Surf. Sci.* **388**, 5–14 (1997).

¹³M. Foss, R. Feidenhans'l, M. Nielsen, E. Findeisen, T. Buslaps, R. I. Johnson, F. Besenbacher, and I. Stensgaard, “Sulfur chemisorption on Ni(111): The clock structure of the $(5\sqrt{3} \times 2)S$ phase,” *Phys. Rev. B* **50**, 8950–8953 (1994).

¹⁴H. Walen, D.-J. Liu, J. Oh, H. Lim, J. W. Evans, C. Aikens, Y. Kim, and P. A. Thiel, “Cu₂S₃ complex on Cu(111) as a candidate for mass transport enhancement,” *Phys. Rev. B* **91**, 045426 (2015).

- ¹⁵S. Rousset, S. Gauthier, O. Siboulet, W. Sacks, M. Belin, and J. Klein, "Scanning-tunneling-microscopy observation of adsorbate-induced two-dimensional step faceting on the S/Cu(111) surface," *Phys. Rev. Lett.* **63**, 1265–1268 (1989).
- ¹⁶K. Motai, T. Hoshizume, H. Lu, D. Jeon, and T. Sakurai, "STM of the Cu(111)1 x 1 surface and its exposure to chlorine and sulfur," *Appl. Surf. Sci.* **67**, 246–251 (1993).
- ¹⁷N. Prince, D. Seymour, M. Aswin, C. F. McConville, and D. P. Woodruff, "A SEXAFS and X-ray standing wave study of the Cu(111) ($\sqrt{7} \times \sqrt{7}$)R 19°-S surface: Adsorbate-substrate and adsorbate-adsorbate registry," *Surf. Sci.* **230**, 13–26 (1990).
- ¹⁸C. T. Campbell and B. E. Koel, "H₂S/Cu(111): A model study of sulfur poisoning of water-gas shift catalysts," *Surf. Sci.* **183**, 100–112 (1987).
- ¹⁹S. M. Driver and D. P. Woodruff, "A new pseudo-(100) sulphur-induced reconstruction of Cu(111) observed by scanning tunnelling microscopy," *Surf. Sci.* **479**, 1–10 (2001).
- ²⁰E. Wahlström, I. Ekwall, H. Olin, S. A. Lindgren, and L. Wallden, "Observation of ordered structures for S/Cu(111) at low temperature and coverage," *Phys. Rev. B* **60**, 10699 (1999).
- ²¹E. Wahlström, I. Ekwall, T. Kihlgren, H. Olin, S. A. Lindgren, and L. Wallden, "Low-temperature structure of S/Cu(111)," *Phys. Rev. B* **64**, 155406 (2001).
- ²²D.-J. Liu, H. Walen, J. Oh, H. Lim, J. W. Evans, Y. Kim, and P. A. Thiel, "Search for the structure of a sulfur-induced reconstruction on Cu(111)," *J. Phys. Chem. C* **118**(50), 29218–29223 (2014).
- ²³C. Wagner, "Investigations on silver sulfide," *J. Chem. Phys.* **21**(10), 1819–1827 (1953).
- ²⁴D. Detry, J. Drowart, P. Goldfinger, H. Keller, and H. Rickert, "Zur thermodynamik von Schwefeldampf," *Z. Phys. Chem.* **55**(5-6), 314–319 (1967).
- ²⁵M. Shen, D.-J. Liu, C. J. Jenks, and P. A. Thiel, "Novel self-organized structure of a Ag-S complex on the Ag(111) surface below room temperature," *J. Phys. Chem. C* **112**(11), 4281–4290 (2008).
- ²⁶I. Horcas, R. Fernandez, J. M. Gomez-Rodriguez, J. Colchero, J. Gomez-Herrero, and A. M. Baro, "WSXM: A software for scanning probe microscopy and a tool for nanotechnology," *Rev. Sci. Instrum.* **78**(1), 013705 (2007).
- ²⁷D.-J. Liu, "Density functional analysis of key energetics in metal homoepitaxy: Quantum size effects in periodic slab calculations," *Phys. Rev. B* **81**, 035415 (2010).
- ²⁸J. Tersoff and D. R. Hamann, "Theory and application for the scanning tunneling microscope," *Phys. Rev. Lett.* **50**(25), 1998–2001 (1983).
- ²⁹M. Shen, C. J. Jenks, J. W. Evans, and P. A. Thiel, "Rapid decay of vacancy islands at step edges on Ag(111): Step orientation dependence," *J. Phys.: Condens. Matter* **22**, 215002 (2010).
- ³⁰S. M. Russell, Y. Kim, D.-J. Liu, J. W. Evans, and P. A. Thiel, "Structure, formation, and equilibration of ensembles of Ag-S complexes on an Ag surface," *J. Chem. Phys.* **138**, 071101 (2013).
- ³¹M. Giesen, "Step and island dynamics at solid/vacuum and solid/liquid interfaces," *Prog. Surf. Sci.* **68**, 1–153 (2001).
- ³²M. Shen, D.-J. Liu, C. J. Jenks, P. A. Thiel, and J. W. Evans, "Accelerated coarsening of Ag adatom islands on Ag(111) exposed to S: Mass-transport mediated by Ag-S complexes," *J. Chem. Phys.* **130**, 094701 (2009).
- ³³See supplementary material at <http://dx.doi.org/10.1063/1.4921258> for tunneling conditions for the STM images presented in the main text.